

Banu Çakırer, DDS, PhD
Assistant Professor
Hacettepe Üniversitesi
Dis Helişligi Fakültesi Ortodonti
Sihhiye, Ankara, Turkey

David Dean, PhD
Assistant Professor
Department of Neurological
Surgery

Juan Martin Palomo, DDS, MSD
Assistant Professor
Department of Orthodontics

**Mark Guenther Hans, DDS,
MSD**
Associate Professor and Chair
Department of Orthodontics

Case Western Reserve University
Cleveland, Ohio

Reprint requests:
Dr Banu Çakırer
Hacettepe Üniversitesi
Dis Helişligi Fakültesi Ortodonti
ABD 06100 Sihhiye, Ankara, Turkey
Fax: ++ 90 312 3091138

Orthognathic surgery outcome analysis: 3-dimensional landmark geometric morphometrics

Traditional cephalometric analysis of 2-dimensional (2D) landmarks has been limited to distances, indices, and angles. Quantitative results vary depending on what baseline is chosen. Geometric morphometric techniques, such as Procrustes superimposition, assume all landmarks carry equivalent information. Using these methods, landmark coordinates (x, y, z) facilitate comparison of patients and "normative" shapes and assessment of pre- to postoperative outcomes. Pre- and postoperative lateral and frontal cephalograms and stereophotograms were taken of a 48-year-old Caucasian man and a 38-year-old Caucasian woman. Coordinates of 3D hard tissue landmarks were collected directly from scanned cephalograms, and 3D soft tissue landmarks were collected onscreen. Procrustes superimpositions of pre- and postoperative 3D craniodental landmark coordinates and 3D soft tissue coordinates were made, and scatter plots were created to show the surgical shape change separately for each patient. Procrustes superimposition of the preoperative and "normative" craniodental data (18-year-old male and female Bolton standards) provided both qualitative and quantitative evaluations of the patients, allowing a better determination of the required treatment. Unlike traditional baseline-dependent methods, Procrustes shape analysis produces a single useful measure of surgical shape change or comparison to normative shape. (Int J Adult Orthod Orthognath Surg 2002;17:xxx-xxx)

The widespread availability of inexpensive 3-dimensional (3D) surface scanning and stereoradiographic imaging presents new opportunities for the planning, execution, and outcome assessment of orthognathic surgery for the correction of dento-facial deformities. 3D landmark localization was inherent in the original presentation of Broadbent's method¹ for the capture and analysis of cephalograms. Biorthogonal lateral and frontal plain-film head radiographs have been a standard 2D adjunct to the planning and assessment of outcome²⁻⁶ of orthognathic surgery for more than 70 years.

Traditional cephalometric 2D interlandmark distances have recently been chal-

lenged^{7,8} as a means for monitoring change resulting from surgery, because the anecdotal methods used for image superimposition create bias, either from time point to time point or from the patient to a standard image, as well as problems of failing to adequately control for size effects.⁹ While they do not suffer from these problems, traditional linear, angular, and proportional measures (indices) have been criticized^{10,11} as an incomplete evaluative basis; these measurements do not adequately represent the shape of interest and do not record positional difference or change.^{5,8,9,12,13} Commonly, different analyses of the same cephalogram may result in different diagnoses, even when appraised

by the same clinician.¹⁴ The failure of maxillofacial practitioners to adopt objective and effective shape measurements, instead preferring anecdotal approaches and diagnostic interpretation, has been shown to result in diagnosis and treatment that varies with the clinician's preferred basis for cephalogram orientation and registration.^{8,12,15–18}

Broadbent¹ originally noted that lateral and frontal cephalograms could be used to obtain 3D data.^{19–23} However, this work is considered impractical by many because it is time consuming,²⁴ may also suffer from lower precision²⁵ than 3D computerized tomography (CT) or 3D magnetic resonance imaging (MRI),^{26–31} and requires complex hardware and software.²⁴ Instead, overlays of manual radiograph tracings are as much a standard of craniofacial practice as they were 50 years ago.

Despite the lack of use, most practitioners recognize that the 3D wireframes produced from biorthogonal 2D cephalograms provide unambiguous information on patient hard tissue anatomy that is otherwise unavailable. Several clinicians have demonstrated the use of 3D landmark localization from biorthogonal cephalograms.^{5,32,33} With the rapid advent of easy-to-use, high-resolution, 3D craniofacial soft tissue,³⁴ dental cast,^{35,36} and skull³⁷ imaging techniques, there is renewed interest in 3D clinical imaging of craniofacial surgery patients. It is now possible to collect 3D coordinate data for soft tissue landmarks and internal hard tissues (bone and teeth) without using expensive CT or 3D MRI.^{26–31} While the internal structures are readily visible in plain-film radiographs, external soft tissue surfaces may be imaged by moire photography,^{38,39} contour photography,⁴⁰ laser scanning systems,^{41–46} or stereophotogrammetry.^{47–52}

The use of landmark data derived from surface images is receiving increased attention,⁵³ because the analysis based on the configuration of landmarks allows one to work with the full geometry of objects, which is otherwise lost. New geometric morphometric techniques, such as Procrustes superimposition (the construction of a 2-form superimposition by a least-squares method^{24,54}), assume all landmarks

carry equivalent information. Procrustes superimposition treats size as a separate variable from shape, preventing it from over-determining the resulting shape analysis. The Procrustes algorithm translates 2D or 3D landmark coordinates of one form as a group to best fit those of a second form.⁵⁵ The fitted object's landmarks are moved to a common center, with the target object's landmarks scaled to a common size and rotated until its landmark coordinates achieve the best approximation of the second object's homologous landmarks.⁵⁴ The rest of the superimposed form is transformed on the basis of this fit, providing an intuitive comparative visualization. Differences in shape are then shown by residual differences (ie, Procrustes distances) in the positions of corresponding landmarks. Using this method, it is possible to measure shape differences between patient and "normative" data for diagnosis or treatment planning, or later, to measure pre- to postsurgical shape change for the outcome assessment. The postoperative data can be Procrustes fit to the "normative" shape for an independent, quantitative measure of the shape change brought about by the surgery. Moreover, if the "normative" shape is the target of the surgery, one would expect that the shape distance of the patient to the normative shape would decrease postoperatively.

The objective of this project was to determine craniofacial hard and soft tissue shape changes that occur following orthognathic surgery and to assess those changes relative to traditional analytic methods and the relevant "Bolton standard" data.

Materials and methods

Cephalograms, 3D soft tissue images, and dental casts were obtained from 2 patients who underwent orthognathic surgery. Patient 1 is a 48-year-old Caucasian man. Patient 2 is a 38-year-old Caucasian woman.

Pre- and postoperative lateral and frontal cephalometric radiographs of these 2 patients were taken using a Broadbent-Bolton roentgenographic cephalometer. The cephalogram radiographs were

Fig 1 The 3dCEPH program^{24,25,56,57} was used to collect 3D coordinates (x, y, z) for 50 craniodental landmarks (see Table 1) by direct digitization of registered biorthogonal plain-film radiographs. This program assumes no movement between the capture of true, orthogonally aligned lateral and frontal cephalograms. For this we use a Broadbent-Bolton roentgenographic cephalometer (see text). This software interface maximizes the interaction between the 2 films so that the user can sight each landmark across both images to most accurately locate its 3D coordinates. Note that the landmarks are not yet in place when initially displayed; the user places them manually in the correct location. The orbital landmarks have not been localized on the frontal image.



scanned on a SCAN-Master DX (Howtek). 3D coordinates of 50 craniodental landmarks were collected by direct digitization of registered biorthogonal plain-film radiographs on a computer using the 3dCEPH program^{56,57} [AU: Manufacturer of 3dCEPH program?] (Fig 1). The development, including accuracy and precision testing, of the 3D landmark localization protocol (Table 1, Figs 2a and 2b) is discussed by Dean et al.²⁵ The mechanism for abstracting 3D hard tissue landmark coordinates has been previously presented.^{24,56,57}

Pre- and postoperative stereophotogrammetric images of patient 1 and patient 2 were taken with a stereophotogrammetric camera (Virtuosa Shape Camera, Visual Interface). 3D coordinates of 65 soft tissue landmarks were collected by direct digitization of stereophotogrammetric images on a computer (Fig 3). The soft tissue landmark localization protocol (Fig 4, Table 2) was developed by David Dean.^{52,58}

Operator precision

Operator precision was tested by redigitizing each pair of biorthogonal cephalograms and each stereophotogrammetric 3D surface image 3 times. The overall Procrustes distance was calculated between all sessions. Procrustes grand means⁵⁴ were generated from these 3 sessions separately for craniodental and soft tissue landmarks (Figs 5 and 6).

Procrustes grand means from all preoperative craniodental and soft tissue landmark digitizing sessions were Procrustes fit to the 3D landmark coordinates of the relevant postoperative craniodental and soft tissue grand means. The superimposition utilized the Procrustes fitting algorithm found in the S-PLUS statistics package (Statsci). Differences in shape were indicated for each landmark as so-called Procrustes distance units (PDUs).^{54,59,60} Landmarks associated with structures unaffected by the surgery, but that showed greater Procrustes distance than points in the area affected by the surgery, were judged to present a lack of localization reliability (ie, imprecision) and were dropped. For symmetric landmark pairs, if only a right or left point was unreliable, the pair was dropped. For patient 1, out of 50 craniodental landmarks, 18 were accepted as reliably localized. Out of 65 soft tissue landmarks, 29 were accepted as reliably localized. For patient 2, 16 craniodental and 30 soft tissue landmarks were found to be reliable.

Shape analysis

Craniodental landmark shape change. Procrustes superimposition of the reliable pre- to postoperative craniodental landmarks was made. Procrustes distance scatter plots were generated to determine the shape change resulting from surgery. The overall Procrustes distance was calculated,

Table 1 Hard tissue 50-landmark protocol*

Landmark no.	Landmark name	Abbreviation
1	Sella	S
2	Basion	Ba
3	Condylion-R	CoR
4	Condylion-L	CoL
5	Mechanical porion-R	PoR
6	Mechanical porion-L	PoL
7	Nasion	N
8	Supraorbital-R	SoR
9	Supraorbital-L	SoL
10	Medial orbit-R	MoR
11	Medial orbit-L	MoL
12	Lateral orbit-R	LoR
13	Lateral orbit-L	LoL
14	Orbitale-R	OrR
15	Orbitale-L	OrL
16	Piriform-R	PiR
17	Piriform-L	PiL
18	Anterior nasal spine	ANS
19	Posterior nasal spine	PNS
20	A point	A
21	Supradentale	Sdl
22	Upper incisor edge	Uie
23	Upper first molar cusp-R	UmR
24	Upper first molar cup-l	Uml
25	Lower incisor edge	Lie
26	Infradentale	Idl
27	Lower first molar cusp-R	LmR
28	Lower first molar cusp-L	LmL
29	B point	B
30	Pogonion	Pog
31	Menton	Me
32	Gonion-R	GoR
33	Gonion-l	GoL
34	Lateral condylar pole-R	LcR
35	Lateral condylar pole-L	LcL
36	Central inc root apex-R	CiR
37	Central inc root apex-L	CiL
38	Ante gonion-R	AgR
39	Ante gonion-L	AgL
40	Opisthion	Opn
41	Opisthocranion	Ocn
42	Inion	Inn
43	Endinion	Edn
44	Glabella	Gl
45	Rhinion	Rhn
46	Mastoidale-R	MsR
47	Mastoidale-L	MsL
48	Euryone-R	EuR
49	Euryone-L	EuL
50	Vertex	Vtx

*See Dean et al²⁵ for definitions and landmark localization protocol.

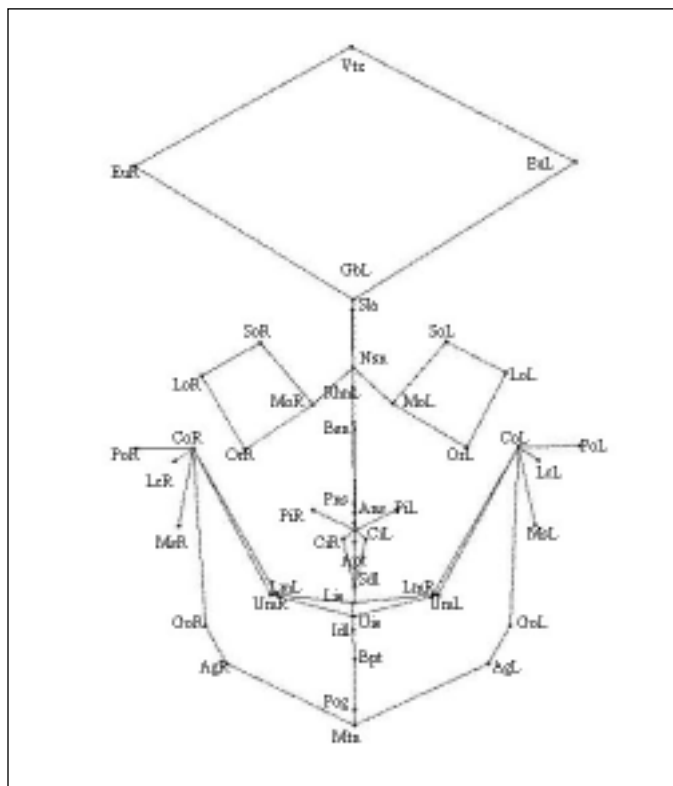


Fig 2a Location of 50 craniodental landmarks, seen from frontal view.

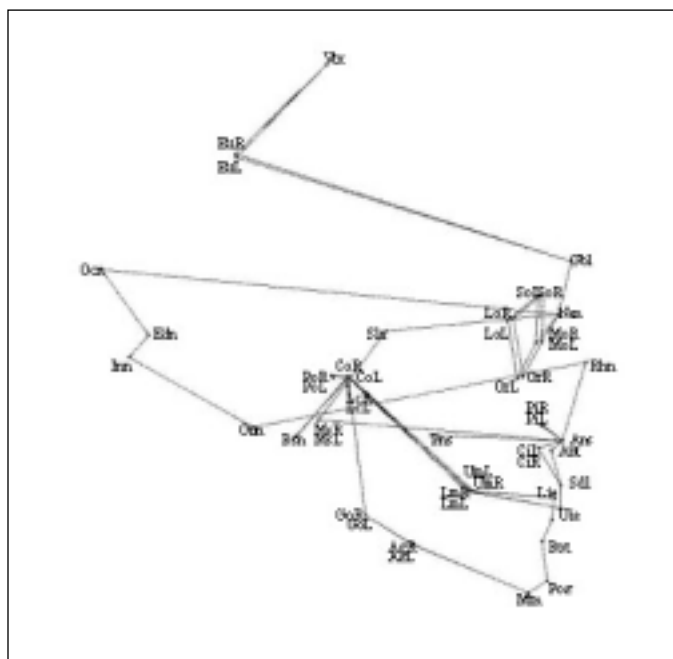


Fig 2b Location of 50 craniodental landmarks, seen from lateral view. Dean et al²⁵ present a full explanation of landmark localization protocol.

Table 2 Soft tissue 50-landmark protocol*

Landmark no.	Landmark name	Abbreviation
1	Glabella	gl
2	Superciliare-R	sci-R
3	Superciliare-L	sci-L
4	Ant frontotemporal-R	aft-R
5	Ant frontotemporal-L	aft-L
6	Palpebrale superius-R	ps-R
7	Palpebrale superius-L	ps-L
8	Endocanthion-R	en-R
9	Endocanthion-L	en-L
10	Exocanthion-R	ex-R
11	Exocanthion-L	ex-L
12	Palpebrale inferius-R	pi-R
13	Palpebrale inferius-L	pi-L
14	Sellion	se
15	Pronasale	prn
16	Alare-R	al-R
17	Alare-L	al-L
18	Subnasale	sn-R [R ok]
19	Labrale superius	ls
20	Labrale superius1-R	ls1-R
21	Labrale superius1-L	ls1-L
22	Cheilion-R	ch-R
23	Cheilion-L	ch-L
24	Stomion	sto
25	Labrale inferius	ls-R
26	Sublabrale	ls-L
27	Pogonion	pog
28	Gnathion	gn
29	Tuberculare-R	tb-R
30	Tuberculare-L	tb-L
31	Gonion-R	go-R
32	Gonion-L	go-L
33	Otobasion inferius-R	obi-R
34	Otobasion inferius-L	obi-L
35	Subaurale-R	sba-R
36	Subaurale-L	sba-L
37	Superaurale-R	sa-R
38	Superaurale-L	sa-L
39	Otobasion superius-R	obs-R
40	Otobasion superius-L	obs-L
41	Tragion-R	t-R
42	Tragion-L	t-L
43	Inferior tragion-R	it-R
44	Inferior tragion-L	it-L
45	Superior antihelix-R	sah-R
46	Superior antihelix-L	sah-L
47	Ant sup med long axis-R	asml-R
48	Ant sup med long axis-L	asml-L
49	Superior lateral tragion-R	slt-R



Fig 3 The 3D coordinates (landmark name and x, y, z columns from left to right in table, right) of the soft tissue landmarks were collected by direct digitization of stereophotogrammetric images (see Table 2).

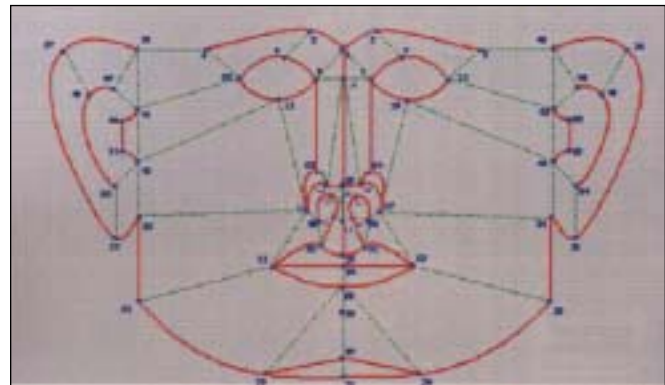


Fig 4 Soft tissue face landmark location map. See Macaraeg⁵⁸ for full key and landmark localization protocol.

Table 2 Cont. Soft tissue 50-landmark protocol*

Landmark no.	Landmark name	Abbreviation
50	Superior lateral tragion-L	silt-L
51	Inferior lateral tragion-R	ilt-R
52	Inferior lateral tragion-L	ilt-L
53	Inferior antihelix-R	ih-R
54	Inferior antihelix-L	ih-L
55	Lateral subalare-R	lsbal-R
56	Lateral subalare-L	lsbal-L
57	Medial subalare-R	msbal-R
58	Medial subalare-L	msbal-L
59	Supra subalare-R	ssbal-R
60	Supra subalare-L	ssbal-L
61	Lateral pronasale-R	lprns-R
62	Lateral pronasale-L	lprns-L
63	Superior alare-R	sal-R
64	Superior alare-L	sal-L
65	Infrapronasale	iprns

*See Macaraeg⁵⁸ for definitions.



Fig 5 Frontal view of 3D landmark wireframe showing the Procrustes grand mean of the craniodental landmarks from 3 different digitizing sessions.



Fig 6 Frontal view of 3D landmark wireframe showing the Procrustes grand mean of the soft tissue landmarks from 3 different digitizing sessions.

as were the Procrustes distances between each corresponding landmark. This shape difference was normalized by dividing each landmark's Procrustes distance by the overall Procrustes distance. This way, the variation in shape attributable to each landmark (ie, normalized PDU) could be expressed as a percentage.

To determine whether the overall shape difference between the patient and "normative" improved following surgery, for patient 1, first, 3D coordinates of reliable preoperative craniodental landmarks were superimposed with the 18-year-old male 3D Bolton standard,²⁴ and the overall Procrustes distance was calculated and scatter plots were generated. Next, 3D coordinates of reliable postoperative craniodental landmarks were superimposed onto the 18-year-old male 3D Bolton standard.²⁴ Procrustes distances were calculated and scatter plots were generated. For patient 2, the same superimpositions, calculations, and scatter plots were made between the patient and the 18-year-old female 3D Bolton standard.²⁴

Soft tissue landmark shape change. To determine the overall soft tissue landmark shape change following surgery, the 3D coordinates of the reliable pre- and postoperative soft tissue landmarks were superimposed via a Procrustes fit and scatter plots were generated. The overall Procrustes distance was calculated, as were the Procrustes distances between each corre-

sponding landmark. The shape difference found at each landmark was normalized by dividing each landmark Procrustes distance by the overall Procrustes distance to produce normalized PDUs.

To determine the soft tissue shape change occurring locally in the areas of the nose, chin, and about the lips, the normalized PDUs of the landmarks in those regions were summed separately.

Results

Patient 1

Craniodental landmarks. The results of the Procrustes superimposition of the pre- and postoperative reliable craniodental landmark 3D coordinates can be seen in Table 3, and scatter plots of the Procrustes fitted landmarks are shown in Fig 7. The overall non-normalized shape difference between pre- and postoperative craniodental landmark sets was 92.562 PDUs. The original and normalized landmark Procrustes distances, from highest to lowest, are listed in Table 3. The highest Procrustes distance indicates the greatest shape change. Normalized distances are calculated to show how much of the overall shape difference is attributable to each landmark. In patient 1, 14.3% of the shape change was attributable to posterior nasal spine, 9.8% to upper incisor edge, 8.1% to central incisor root apex-left, 7.4% to cen-

Fig 7 Scatter plots of the Procrustes superimposition of preoperative (Rprhmeanrel) and postoperative (Rpohmeanrel) reliable craniodental landmarks for patient 1, a 48-year-old male undergoing palatal advancement (see Table 3).

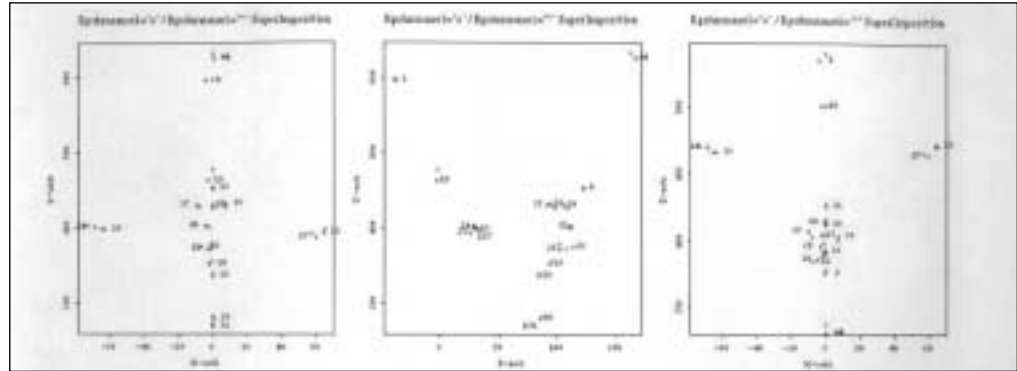


Table 3 Procrustes superimposition of reliable craniodental landmarks from the pre- to postoperative condition in patient 1

Rank	Landmark	PDU	Normalized PDU
1	Posterior nasal spine (19)	13.267	.143
2	Upper incisor edge (22)	9.098	.098
3	Central inc root apex-L (37)	7.504	.081
4	Central inc root apex-R (36)	6.828	.074
5	A point (20)	6.811	.074
6	Glabella (44)	6.602	.071
7	Upper first molar-L (24)	5.019	.054
8	Sella (1)	4.980	.054
9	Lower incisor edge (25)	4.957	.054
10	Upper first molar-R (23)	4.458	.048
11	Lower first molar-R (27)	4.103	.044
12	Supradentale (21)	3.949	.043
13	Anterior nasal spine (18)	3.785	.041
14	Lower first molar-L (28)	3.450	.037
15	Infradentale (26)	3.000	.032
16	Pogonion (30)	1.944	.021
17	Menton (31)	1.447	.016
18	B point (29)	1.360	.015
Overall Procrustes distance		92.562	

tral incisor root apex-right, and 7.4% to A point.

The hard tissue landmark analysis included superimposition of the patient's pre- and postoperative landmark data to the average 18-year-old male Bolton standard.²⁴ Overall Procrustes distance and the Procrustes distance at each landmark and related scatter plots are presented in Tables 4 and 5 and Figs 8 and 9, respectively. The preoperative to 18-year-old male 3D Bolton standard overall Procrustes distance was found to be 200.4 PDUs. The Pro-

crustes superimposition of the 18-year-old male Bolton standard to the postoperative data produced an overall Procrustes distance of 193.9 PDUs. Thus, the overall shape difference between the patient and the 3D Bolton standard decreased 3.4% postsurgically at these 18 landmarks.

Soft tissue landmarks. The overall Procrustes distance between pre- and postoperative soft tissue landmark sets was 98.797 PDUs (Table 6, Fig 10). Gonion-L was found to be responsible for 6.9% of overall shape change. When we grouped the land-

Table 4 Procrustes superimposition of the average 18-year-old male Bolton standard reliable craniodental landmarks to the preoperative condition in patient 1			
Rank	Landmark	PDU	Normalized PDU
1	Anterior nasal spine (18)	17.526	.087
2	Supradentale (21)	14.999	.075
3	Lower first molar-R (27)	14.857	.074
4	Pogonion (30)	13.437	.067
5	Lower incisor edge (25)	12.884	.064
6	Lower first molar-L (28)	11.857	.059
7	Glabella (44)	11.813	.059
8	Upper first molar-L (24)	11.635	.058
9	Upper incisor edge (22)	11.006	.055
10	A point (20)	10.608	.053
11	Infradentale (26)	10.402	.052
12	Central root apex-L (37)	10.325	.052
13	Sella (1)	10.238	.051
14	Menton (31)	10.163	.051
15	Posterior nasal spine (19)	9.691	.048
16	Upper first molar-R (23)	7.849	.039
17	Central root apex-R (36)	6.489	.032
18	B point (29)	4.667	.023
Overall Procrustes distance		200.446	

Table 5 Procrustes superimposition of the average 18-year-old male Bolton standard reliable craniodental landmarks to the postoperative condition in patient 1			
Rank	Landmark	PDU	Normalized PDU
1	Glabella (44)	15.701	.081
2	Anterior nasal spine (18)	14.912	.077
3	Posterior nasal spine (19)	14.476	.075
4	Lower first molar-R (27)	14.450	.075
5	Supradentale (21)	13.359	.069
6	Lower first molar-L (28)	13.345	.069
7	Pogonion (30)	11.430	.059
8	Upper first molar-L (24)	10.905	.056
9	Central inc root apex-L (37)	10.402	.054
10	Lower incisor edge (25)	9.862	.051
11	Central inc root apex-R (36)	9.742	.050
12	Upper first molar-R (23)	9.735	.050
13	Upper incisor edge (22)	9.670	.050
14	Menton (31)	8.755	.045
15	A point (20)	8.313	.043
16	Infradentale (26)	8.265	.043
17	Sella (1)	6.127	.032
18	B point (29)	4.482	.023
Overall Procrustes distance		193.931	

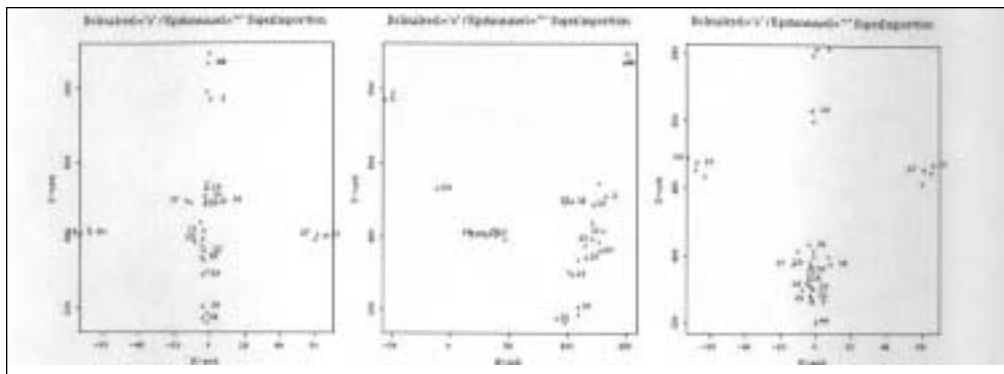


Fig 8 Scatter plots of the Procrustes superimposition of the average 18-year-old male Bolton standard (Bolmalere) and preoperative (Rphmeanrel) craniodental landmarks for patient 1 (see Table 4).

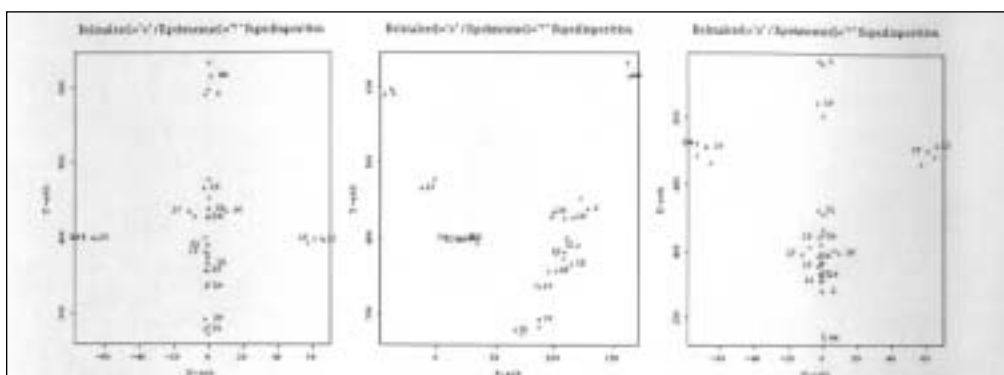


Fig 9 Scatter plots of the average 18-year-old male Bolton standard (Bolmalere) and postoperative (Rphmeanrel) craniodental landmarks for patient 1 (see Table 5).

Table 6 Procrustes superimposition of reliable soft tissue landmarks from pre- to postoperative condition in patient 1

Rank	Landmark	PDU	Normalized PDU
1	Gonion-L (32)	6.840	.069
2	Superior alare-L (38)	6.588	.067
3	Pogonion (27)	6.574	.067
4	Alare-L (17)	5.989	.061
5	Tuberculare-L (30)	5.951	.060
6	Gonion-R (31)	5.659	.057
7	Cheilion-L (23)	4.874	.049
8	Cheilion-R (22)	3.850	.039
9	Superior alare-R (37)	3.826	.039
10	Supra subalare-L (60)	3.803	.038
11	Sublabale (26)	3.606	.036
12	Lateral subalare-L (56)	3.577	.036
13	Infrapronasale (65)	3.313	.034
14	Gnathion (28)	3.270	.033
15	Supra subalare-R (59)	3.155	.032
16	Labrale superius1-L (21)	3.057	.031
17	Labrale superius1-R (20)	2.680	.027
18	Lateral pronasale-R (61)	2.627	.027
19	Lateral pronasale-L (62)	2.513	.025
20	Labriale superius (19)	2.469	.025
21	Medial subalare-L (58)	2.160	.022
22	Labriale inferius (25)	1.888	.019
23	Subnasale (18)	1.877	.019
24	Pronasale (15)	1.852	.019
25	Medial subalare-R (57)	1.742	.018
26	Stomion (24)	1.612	.016
27	Lateral subalare-R (55)	1.532	.016
28	Tuberculare-R (29)	1.624	.016
29	Alare-R (16)	0.2889	.003
Overall Procrustes distance		98.797	

Fig 10 Scatter plots of the Procrustes superimposition of preoperative (Rprsmearrel) and postoperative (Rposmeanrel) soft tissue landmarks for patient 1 (see Table 6).

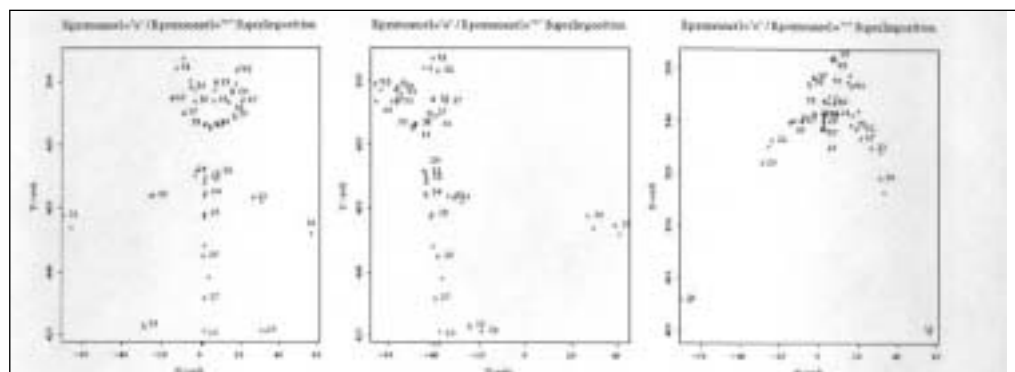


Table 7		Procrustes superimposition of reliable craniodental landmarks from the pre- to postoperative condition in patient 2	
Rank	Landmark	PDU	Normalized PDU
1	Lower first molar-L (28)	10.039	.12
2	Lower first molar-R (27)	9.991	.12
3	Posterior nasal spine (19)	6.491	.08
4	B point (29)	5.718	.07
5	A point (20)	5.703	.07
6	Infradentale (26)	5.658	.07
7	Upper incisor edge (22)	5.616	.07
8	Supradentale (21)	5.571	.06
9	Central inc root apex-L (37)	5.529	.06
10	Lower incisor edge (25)	5.238	.06
11	Upper first molar-L (24)	5.208	.06
12	Central inc root apex-R (36)	4.551	.05
13	Anterior nasal spine (18)	3.373	.04
14	Upper first molar-R (23)	3.153	.04
15	Menton (31)	3.037	.04
16	Pogonion (30)	1.236	.01
Overall Procrustes distance		86.114	

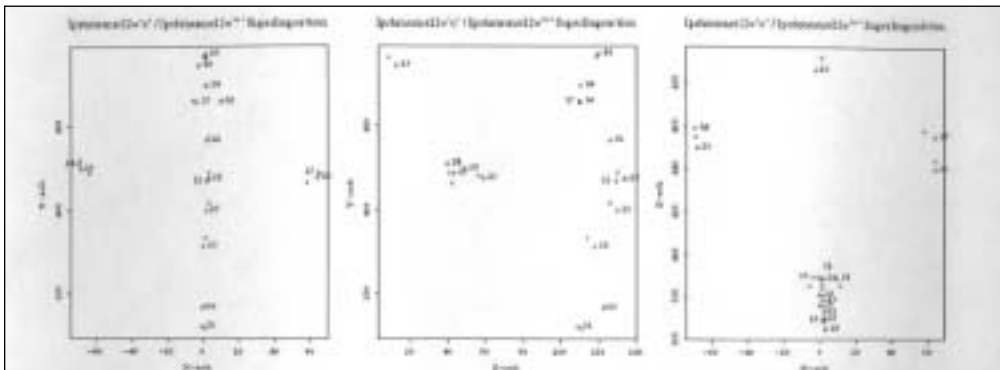


Fig 11 Scatter plots of the superimposition of preoperative (Iprhmeanrel) and postoperative (Ipohmearel) craniodental landmarks for patient 2, a 38-year-old female undergoing palatal advancement (see Table 7).

marks as chin, lips, and nose, it was found that 45.6% of the shape change was attributable to the nose area, followed by 31.9% in the chin area and 24.2% about the lips.

Patient 2

Craniodental landmarks. The overall shape difference between pre- and postoperative craniodental landmark sets was 86.114 PDUs (Table 7, Fig 11). The landmarks are listed in descending order from highest to lowest PDU. Normalized distances were also calculated to show how much of the overall difference was attributable to each landmark; 12% of the shape

change was attributable to lower first molar-L, 12% to lower first molar-R, 8% to posterior nasal spine, 7% to B point, 7% to A point, 7% to infradentale, and 7% to upper incisor edge.

The analysis of patient 2 was also extended to include superimposition of both the pre- and postoperative landmarks to the 3D coordinates of the average 18-year-old female Bolton standard data²⁴ (Tables 8 and 9 and Figs 12 and 13, respectively). The overall Procrustes distance between the 18-year-old female 3D Bolton standard and the patient's preoperative measurements was 145.4 PDUs. The Procrustes superimposition of the 18-year-old female Bolton

Table 8		Procrustes superimposition of the average 18-year-old female Bolton standard reliable craniodental landmarks to the preoperative condition in patient 2	
Rank	Landmark	PDU	Normalized PDU
1	Upper first molar-R (23)	18.239	.13
2	Anterior nasal spine (18)	17.145	.12
3	Posterior nasal spine (19)	14.333	.10
4	A point (20)	13.773	.09
5	Lower incisor edge (25)	11.410	.08
6	Lower first molar-L (28)	11.184	.08
7	Central inc root apex-L (37)	9.045	.06
8	Lower first molar-R (27)	8.062	.06
9	Upper first molar-L (24)	7.856	.05
10	Central inc root apex-R (36)	7.491	.05
11	Supradentale (21)	7.281	.05
12	Infradentale (26)	6.689	.05
13	Upper incisor edge (22)	5.276	.04
14	Pogonion (30)	4.768	.03
15	Menton (31)	1.622	.01
16	B point (29)	1.227	.01
Overall Procrustes distance		145.401	

Table 9		Procrustes superimposition of the average 18-year-old female Bolton standard reliable craniodental landmarks to the postoperative condition in patient 2	
Rank	Landmark	PDU	Normalized PDU
1	Anterior nasal spine (18)	16.187	.13
2	Upper first molar-R (23)	14.655	.12
3	Posterior nasal spine (19)	12.742	.10
4	Central inc root apex-L (37)	10.099	.08
5	Lower first molar-R (27)	9.541	.08
6	Lower first molar-L (28)	9.022	.07
7	Central inc root apex-R (36)	8.767	.07
8	A point (20)	8.235	.07
9	Upper first molar-L (24)	7.441	.06
10	Lower incisor edge (25)	5.730	.05
11	B point (29)	5.181	.04
12	Supradentale (21)	5.159	.04
13	Upper incisor edge (22)	4.347	.03
14	Pogonion (30)	3.775	.03
15	Menton (31)	2.864	.02
16	Infradentale (26)	2.725	.02
Overall Procrustes distance		126.47	

Fig 12 Scatter plots of the Procrustes superimposition of the average 18-year-old female Bolton standard (Bolfemalere1) and preoperative craniodental landmarks (lprhmeanrel2) for patient 2 (see Table 8).

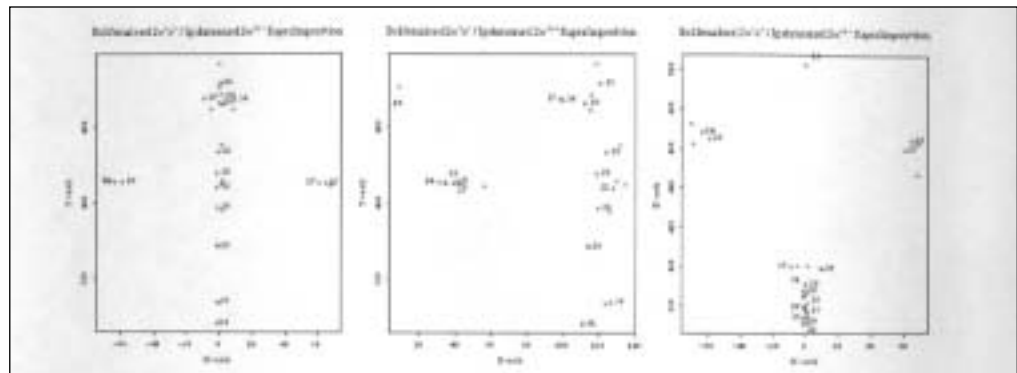


Fig 13 Scatter plots of the Procrustes superimposition of the average 18-year-old female Bolton standard (Bolfemalere1) and postoperative craniodental landmarks (lpohmeanrel2) for patient 2 (see Table 9).

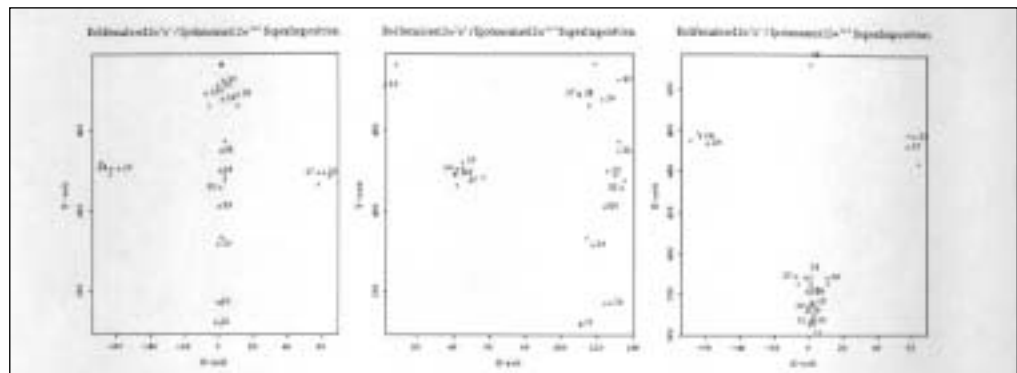


Table 10		Procrustes superimposition of reliable soft tissue landmarks from pre- to postoperative condition in patient 2	
Rank	Landmark	PDU	Normalized PDU
1	Gonion-L (32)	5.597	.07
2	Labrale superius 1-R (20)	5.402	.06
3	Labrale superius1-L (21)	4.908	.06
4	Tuberculare-L (30)	4.691	.05
5	Gnathion (28)	4.365	.05
6	Alare-L (17)	4.336	.05
7	Sellioin (14)	3.880	.05
8	Labrale superius (19)	3.573	.04
9	Lateral subalare-R (55)	3.444	.04
10	Labrale inferius (25)	3.354	.04
11	Alare-R (16)	3.325	.04
12	Supr subalare-L (60)	3.323	.04
13	Cheilion-L (23)	3.29	.04
14	Stomion (24)	2.707	.03
15	Cheilion-R (22)	2.674	.03
16	Lateral pronasale-L (62)	2.640	.03
17	Sublabrale (26)	2.617	.03
18	Tuberculare-R (29)	2.424	.03
19	Supra subalare-R (59)	2.373	.03
20	Infrapronasale (65)	2.259	.03
21	Gonion-L (32)	2.142	.02
22	Medial subalare-R (57)	1.964	.02
23	Medial subalare-L (58)	1.731	.02
24	Superaurale-R (37)	1.713	.02
25	Superaurale-L (38)	1.683	.02
26	Lateral pronasale-R (61)	1.675	.02
27	Subnasale (18)	1.278	.01
28	Pronasale (15)	0.928	.01
29	Pogonion (27)	0.882	.01
30	Lateral subalare-L (56)	0.786	.01
Overall Procrustes distance		85.971	

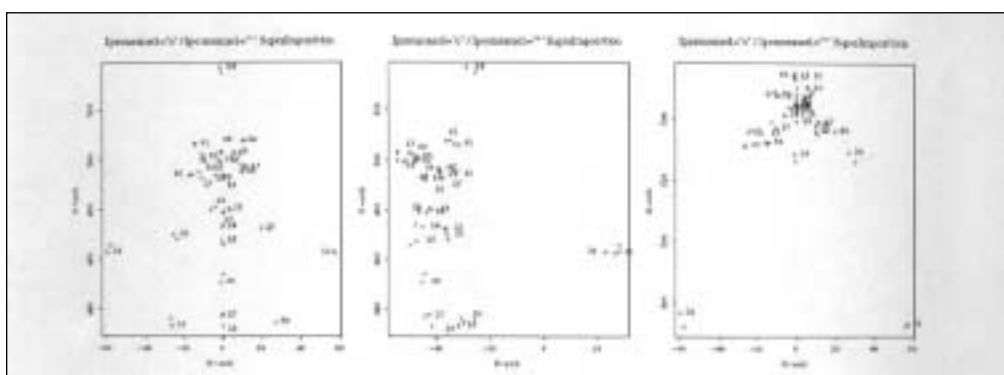


Fig 14 Scatter plots of the Procrustes superimposition of preoperative (lprsmearrel) and postoperative (lposmeanrel) soft tissue landmarks for the Case 2 patient (see Table 10).

standard to the postoperative data produced an overall Procrustes distance of 126.5 PDUs. Thus, the overall shape difference between the patient and 3D Bolton standard decreased 12.9% postsurgically at these 16 landmarks.

Soft tissue landmarks. Soft tissue shape change related to the orthognathic surgery was also judged via Procrustes superimposition between the 3D coordinates of the 30 reliable soft tissue pre- and postoperative landmark sets. Scatter plots were created (Table 10, Fig 14). The overall Procrustes distance between these 2 data sets was 85.97 PDUs. Gonion-R was responsible for 7% of this overall change. When we grouped the landmarks as chin, mouth, and nose, it was found that 43.4% of the shape change was attributable to the nose area, followed by 33.1% about the lips and 23.3% in the chin area.

Discussion

As the Procrustes approach becomes more established, its application to various biologic disciplines is becoming increasingly widespread. Examples of studies making use of these methods can be found in many fields, from zoology to medicine.⁶¹⁻⁶⁴

This paper examined craniofacial hard and soft tissue shape changes that occur following orthognathic surgery and assessed those changes relative to traditional analytic methods and the relevant "Bolton standard" data. As with any other method of analysis, successful implementation depends on the accuracy and reliability with which data (eg, landmark locations) are collected. Our first task was to demonstrate that our localization of landmarks demonstrated adequate precision. Precision is the inverse of the variation between multiple estimates of the same quantity—in this case, landmark localization. Without information on precision, it would be difficult to dissect shape difference from localization error.⁶⁵⁻⁷⁴ Moreover, precision tests allow the operator to determine when they are adequately trained in the landmark localization protocol and can begin collecting patient data.

Operator precision was tested by redigitizing biorthogonal cephalograms and

stereophotogrammetric images 3 times. The biorthogonal plain-film radiographic reconstruction of the hard tissue landmarks proved less reliable than the stereophotogrammetric reconstruction of soft tissue landmarks. This finding was expected from our earlier work comparing 3D cephalogram and 3D CT surface image landmark localization precision.²⁵ The presence of color in soft tissue stereophotograms seems to increase localization precision.⁷⁵

It is disturbing that different landmark sets are less reliable in different biorthogonal cephalogram pairs, whereas the reliability of stereophotogram landmarks is consistent. The 3dCEPH software implementation of the Broadbent Orientator increases precision through simultaneous sighting of landmarks aligned in both the frontal and lateral cephalograms.⁵⁶ This method improves precision over separate identification of each landmark on the lateral and frontal tracings via a digitizing tablet.^{32,76} However, at least 3 factors may prevent the x-ray beams that produce biorthogonal cephalograms from intersecting accurately.²² First, there is a concentric beam spreading away from the central ray in both the frontal and lateral images. This effect is corrected by the Broadbent Orientator⁷⁷ and tracked in the 3dCEPH program. Second, it is difficult to verify that the patient's head is truly in Frankfort orientation in the Broadbent-Bolton roentgenographic cephalometer^{1,24}; however, a more pressing problem for 3D landmark localization accuracy is to insure that a consistent position is held when the frontal and lateral views are obtained. This is very difficult to insure when the patient is turned orthogonally in front of a single, unregistered x-ray aperture, a method that is commonly employed to save space over the Broadbent-Bolton roentgenographic cephalometer. Finally, head movements that occur, perhaps inadvertently, between taking the frontal and lateral films can greatly affect 3D accuracy⁷³ and comparisons of landmarks taken at 2 time points.

Following the precision study, we tested the hypothesis that quantitative landmark shape analysis of facial morphology would be useful at 3 different stages of orthognathic surgical patient care: diagnosis,

treatment planning, and outcome assessment. In this study, 3D Procrustes superimposition, a geometric morphometric technique,⁵⁴ was used because it does not elevate the importance of any one landmark over any other during superimposition and eliminates confounding effects introduced by size differences between compared shapes.⁶²

Procrustes superimposition of the preoperative and "normative" craniodental data (18-year-old male or female Bolton standards) at each corresponding landmark (Tables 4 and 8) supplies clinicians with quantitative data that they can choose to use in their plan for therapy. The objectives of surgery are never to obtain identical results or to correct every patient to the same appearance. However, the assessment of patients at a clinical level takes years of experience, and this current technique may enable all clinicians to quantitatively assess their work as they acquire clinical experience.

The esthetic outcome of an orthognathic procedure has always been an important aspect in the judgment of treatment success by both the clinician and the patient.⁷⁹ Current surgical procedures attempt to re-establish functional and esthetic anatomy by repositioning displaced skeletal elements or by grafting and contouring abnormal bony contours. Principally, soft tissue changes result from these skeletal alterations.⁸⁰

For both patients, the results of the Procrustes superimposition of craniodental landmarks show shape change is greatest in the surgically modified element, the palate. Affected by this maxillary advancement, the nose area showed the greatest shape change in the soft tissue landmarks in both cases. This supports the expected close correlation thought to exist between soft tissue landmarks of the nose and the underlying skeletal and dental structures of the palate.⁸¹

During 6 months of treatment of Class III malocclusions with maxillary expansion and protraction, Ngan et al⁸² found that forward movement of the maxilla was accompanied by 50% to 70% forward movement of the soft tissue profile. However, in the study of interrelationships of the soft

tissue and dentoskeletal profiles, size plays a distorting role because it can mask shape change.⁸³⁻⁸⁷ Geometric morphometrics, such as Procrustes superimposition,⁵⁴ allow assessment of shape change in isolation from the potentially confounding effects of size change.^{88,89} Traditionally, changes in the nose and lip areas would be projected and measured only as seen in the midsagittal plane. However, surgeons, orthodontists, and patients are more concerned about changes in their frontal appearance due to surgery. With 3D coordinates, parasagittal shape change, including the frontal appearance, may also be tracked.

Comparison of the patient and normative hard tissue data (ie, 18-year-old male or female 3D Bolton standards) provides another indication of the direction and amount of shape change resulting from surgery. Indeed, these "normative" data provide a baseline against which patients with the same diagnosis, receiving the same treatment, can be compared before and after surgery to independently determine the amount and direction of shape change. In the 2 cases shown here, the surgical procedure resulted in greater conformity with the appropriate 3D Bolton standard data. The 3D Bolton standard soft tissue landmarks have recently been generated⁵⁸ but were not used in this analysis due to their sparse coverage of the face.

The relative usefulness of individual morphometric procedures is an area of intensive debate.⁹⁰ For example, valid arguments have been presented indicating that shape analyses that compare sets of homologous landmarks depend upon the landmarks selected as well as on the interpolation function used.^{59,91,92} However, it would appear that each technique can provide useful information. The evaluation of cephalometric radiographs might supply sufficient information for treatment planning and outcome assessment when a symmetric or nearly symmetric craniofacial situation is being projected. Unfortunately, a number of orthodontic patients do not have such ideal relationships; these cases could be better treated with a more complete 3D analysis.⁸⁴ Ultimately, Procrustes superimposition, the morphometric technique used in the present study, provides

information on overall facial and cranio-dental shape change resulting from surgery that traditional cephalometrics cannot provide. This additional information can assist the orthodontist and orthognathic surgeon with treatment planning and/or surgical outcome assessment.

Acknowledgment

This project was partially supported by a NATO B1 post-doctoral research scholarship to Banu Çakırer and a Whitaker Foundation Grant to David Dean. We wish to thank Dr Holly Broadbent Jr, Director, Bolton-Brush Growth Study Center, for access to the 3D Bolton standard data. The writers would like to thank Pengpeng Zhang, MSc, for assistance in handling the data.

References

- Broadbent BH. A new x-ray technique and its application to orthodontia. *Angle Orthod* 1931;1:45–69.
- Peppersack WJ, Chausse JM. Long term follow up of the sagittal splitting technique for correction of mandibular prognathism. *J Maxillofac Surg* 1978;6:117–140.
- Nakajima T, Kajikawa Y, Tokiwa N, Hanada K. Stability of mandible after surgical correction of skeletal Class III malocclusion in 50 patients. *J Oral Surg* 1979;37:21–25.
- Kobayashi T, Watanabe I, Ueda K, Nakajima T. Stability of the mandible after sagittal ramus osteotomy for correction of prognathism. *J Oral Maxillofac Surg* 1986;44:693–697.
- Grayson BH. Cephalometric analysis for the surgeon. *Clin Plast Surg* 1989;16:633–644.
- Kobayashi T, Ueda K, Honma K, Sasakura H, Hanada K, Nakajima T. Threedimensional analysis of facial morphology before and after orthognathic surgery. *J Craniomaxillofac Surg* 1990;18:68–73.
- Rubin RM. Making sense of cephalometrics. *Angle Orthod* 1997;67:83–85.
- Moyers RE, Bookstein FL. The inappropriateness of conventional cephalometrics. *Am J Orthod* 1979;75:599–617.
- Fine MB, Lavelle CLB. Diagnoses of skeletal form on the lateral cephalogram with a finite element-based expert system. *Am J Orthod Dentofac Orthop* 1992;101:318–329.
- Savara BS. A method for measuring facial bone growth in three dimensions. *Hum Biol* 1965;37:245–255.
- Baumrind S, Frantz RC. The reliability of head film measurements: 2. Conventional angular and linear measures. *Am J Orthod* 1971b;60:505–517.
- Richtsmeier JT, Cheverud JM. Finite element scaling analysis of human craniofacial growth. *J Craniofac Genet Dev Biol* 1986;6:289–323.
- Lestrel PK. Some approaches toward the mathematical modeling of the craniofacial complex. *J Craniofac Genet Dev Biol* 1989;9:77–91.
- Wylie GA, Fish LC, Epker BN. Cephalometrics: A comparison of five analyses currently used in the diagnosis of dentofacial deformities. *Int J Adult Orthod Orthognath Surg* 1987;2:15–36.
- Rickets RM. New perspectives on orientation and their benefits to clinical orthodontics. Part I. *Angle Orthod* 1975;45:238–248.
- Rickets RM, Schulhof RJ, Bagha L. Orientation—Sella-nasion or Frankfort horizontal. *Am J Orthod* 1976;69:648–654.
- Tng TTH, Chan TCK, Cooke MS, Hägg U. Effect of head posture on cephalometric sagittal angular measures. *Am J Orthod Dentofac Orthop* 1993;104:337–341.
- Murray TM. The pitfalls and merits of using commonly accepted orthodontic cephalometric analyses. *J Gen Orthod* 1997;8:6–17.
- Baumrind S, Moffitt FH, Curry S. Three dimensional x-ray stereometry from paired coplanar images: A progress report. *Am J Orthod* 1983a;84:292–312.
- Baumrind S, Moffitt FH, Curry S. The geometry of three-dimensional measurement from paired coplanar x-ray images. *Am J Orthod* 1983b;84:313–322.
- Grayson B, Cutting C, Bookstein FL, Kim H, McHarty JG. The three-dimensional cephalogram: Theory, technique, and clinical application. *Am J Orthod Dentofac Orthop* 1988;94:327–337.
- Brown T, Abbott AH. Computer-assisted location of reference points in three-dimensions for radiographic cephalometry. *Am J Orthod Dentofac Orthop* 1989;95:490–498.
- Bookstein FL, Grayson B, Cutting CB, Kim H-C, McHarty JG. Landmarks in three dimensions: Reconstruction from cephalograms versus direct observation. *Am J Orthod Dentofac Orthop* 1991a;100:133–140.
- Dean D, Hans MG, Bookstein FL, Subramanyan K. Three-dimensional Bolton-Brush Growth Study landmark data: Ontogeny and sexual dimorphism of the Bolton Standards Cohort. *Cleft Palate Craniofac J* 2000;37:145–156.
- Dean D, Palomo M, Subramanyan K, et al. Accuracy and precision of 3D cephalometric landmarks from biorthogonal plain film x-rays. In: Kim Y, Mun SK (eds). *Medical Imaging 1998, Image Display*, 22–24 February 1998, San Diego, California, vol 3335. Bellingham, WA: International Society for Optical Engineering, 1998:50–58.
- Hounsfield GN. Computerized transverse axial scanning (tomography) 1. Description of system. *Br J Radiol* 1973;46:1016–1022.
- Zonnefeld FW, Lobregt S, van der Meulen JCH, Vaandrager JM. Three-dimensional imaging in craniofacial surgery. *World J Surg* 1989;13:328–342.
- Kreiborg S, Marsh JL, Cohen MM Jr, et al. Comparative three-dimensional analysis of CT-scans of the calvaria and cranial base in Apert and Crouzon syndromes. *J Craniomaxillofac Surg* 1993;21:181–188.
- McCance AM, Moss JP, Fright WR, James DR, Linney AD. A three dimensional analysis of soft and hard tissue changes following bimaxillary orthognathic surgery in skeletal III patients. *Br J Oral Maxillofac Surg* 1992;30:305–312.
- Bettega G, Chenin M, Sadek H, et al. Threedimensional fetal cephalometry. *Cleft Palate Craniofac J* 1996;33:463–467.
- Binaghi S, Gudinchet F, Rilliet B. Three-dimensional spiral CT of craniofacial malformations in children. *Pediatr Radiol* 2000;30:856–860.

32. Cutting CB, Bookstein FL, Grayson B, Fellingham L, McCarthy JG. Three dimensional computer assisted design of craniofacial surgical procedures: Optimization and interaction with cephalometric and CT-based models. *Plast Reconstr Surg* 1986;77:877–885.
33. Kobayashi T, Ueda K, Honma K, Sasakura H, Hanada K, Nakajima T. Three-dimensional analysis of facial morphology before and after orthognathic surgery. *J Craniomaxillofac Surg* 1990;18:68–73.
34. Cutting CB, Dean D, Bookstein FL, Haddad B, Khorramabadi D, Zonneveld F. A three-dimensional smooth surface analysis of untreated Crouzon's Syndrome in the adult. *J Craniofac Surg* 1995;6:444–453.
35. Rekow D. Computer-aided design and manufacturing in dentistry: A review of the state of the art. *J Prosthet Dent* 1987;58:512–516.
36. Berkowitz S. A multicenter retrospective 3D study of serial complete unilateral cleft lip and palate and complete bilateral cleft lip and palate casts to evaluate treatment: Part 1—The participating institutions and research aims. *Cleft Palate Craniofac J* 1999;36:413–424.
37. Dean D, Bookstein FL, Kunero S, Lee JH, Cutting CB, Hans M, Goldberg J. Average African-American 3D-CT images: The clinical importance of ethnicity and sex. *J Craniofac Surg* 1998a;9:348–358.
38. Kawai T, Natsume N, Shibata H, Yamamoto T. Three-dimensional analysis of facial morphology using moire stripes. Part I. Method. *Int J Oral Maxillofac Surg* 1990;19:356–358.
39. Kawai T, Natsume N, Shibata H, Yamamoto T. Three-dimensional analysis of facial morphology using moire stripes. Part II. Analyses of normal adults. *Int J Oral Maxillofac Surg* 1990;19:359–362.
40. Robertson NRE. Contour photography. *Br J Orthod* 1976;3:105–109.
41. Moss JP, Linney AD, Grindrod SR, Arridge SR, Clifton JS. Three-dimensional visualization of the face and skull using computerized tomography and laser scanning techniques. *Eur J Orthod* 1987;9:247–253.
42. Coombes AM, Moss JP, Linney AD, Richards R, James DR. A mathematical method for the comparison of three-dimensional changes in the facial surface. *Eur J Orthod* 1991;13:95–110.
43. Chen L-H, Tsutsumi S, Hyo Y, Lizuka T. A rapid three-dimensional measurement system for facial morphology by laser multi-slits. *Int J Prosthodont* 1993;6:573–578.
44. Moss JP, McCance AM, Fright WR, Linney AD, James DR. A three-dimensional soft tissue analysis of fifteen patients with Class II, Division I malocclusions after bimaxillary surgery. *Am J Orthod Dentofac Orthop* 1994;105:430–437.
45. Duffy S, Noar JH, Evans RD, Sanders R. Three-dimensional analysis of the child cleft face. *Cleft Palate Craniofac J* 2000;37:137–144.
46. Soncul M, Bamber MA. The optical surface scan as an alternative to the cephalograph for soft tissue analysis for orthognathic surgery. *Int J Adult Orthod Orthognath Surg* 1999;14:277–283.
47. Burke PH, Banks P, Beard LFH, Tee JE, Hughes C. Stereophotographic measurement of change in facial soft tissue morphology following surgery. *Br J Oral Surg* 1983;21:237–245.
48. Motoyoshi M, Namura S, Arai HY. A three-dimensional measuring system for the human face using three-directional photography. *Am J Orthod Dentofac Orthop* 1992;101:431–40.
49. Ras F, Habets LLMH, van Ginkel FC, Prah-Anderesen B. Method for quantifying facial asymmetry in three dimensions using stereophotogrammetry. *Angle Orthod* 1995a;65:233–239.
50. Ras F, Habets LLMH, Van Ginkel FC, Prah-Anderesen B. Longitudinal study on three-dimensional changes of facial asymmetry in children between 4 to 12 years of age with unilateral cleft lip and palate. *Cleft Palate Craniofac J* 1995b;32:463–468.
51. Ras F, Habets LLMH, van Ginkel, Prah-Anderesen B. Quantification of facial morphology using stereophotogrammetry—Demonstration of a new concept. *J Dent* 1996;24:369–374.
52. Hans MG, Palomo JM, Dean D, Cakirer B, Min KT, Han S, Broadbent BH. Threedimensional imaging—The CWRU method. *Semin Orthod* 2001;7:233–243.
53. Bacher M, Bacher U, Goz G, et al. Three-dimensional computer morphometry of the maxilla and face in infants with Pierre Robin sequence—A comparative study. *Cleft Palate Craniofac J* 2000;37:292–302.
54. Rohlf FJ, Slice D. Extensions of the Procrustes method for optimal superimposition of landmarks. *Syst Zool* 1990;39:40–59.
55. Robinson DL, Blackwell PG, Stillman EC, Brook AH. Planar Procrustes analysis of tooth shape. *Arch Oral Biol* 2001;46:191–199.
56. Subramanyan K, Dean D. Scanned bi-orthogonal radiographs as a source for 3D cephalometric data. *SPIE* 1996;2710:717–724.
57. Dean D, Subramanyan K, Kim E-K. New Bolton standards: Co-registration of bi-plane x-rays and 3D CT. *SPIE* 1997;3034:541–549.
58. Macaraeg OA. Three-dimensional Changes in the Soft Tissue Face of Ten Bolton Study Males as Seen in Biorthogonal Cephalograms and 3D CT Images [thesis]. Cleveland, OH: Department of Anatomy, Case Western Reserve University, 1996.
59. Bookstein FL. *Morphometric Tools for Landmark Data*. Cambridge: Cambridge University Press, 1991.
60. Goodall CR. Procrustes methods in the statistical analysis of shape. *J R Stat Soc* 1991;B53:285–339.
61. Kingenburgh CP, Bookstein FL (eds). [AU: Title??] *Acta Zool Sci Hung* 1998;44(1–2):1–194.
62. Singh GD, McNamara JA Jr, Lozanoff S. Morphometry of the cranial base in subjects with Class III malocclusion. *J Dent Res* 1997;76:694–703.
63. Singh GD, McNamara JA Jr, Lozanoff S. Comparison of mandibular morphology in Korean and European-American children with Class III malocclusions using Finite element morphometry. *J Orthod* 2000;27:135–142.
64. Singh GD, McNamara JA Jr, Lozanoff S. Finite-element morphometry of soft tissue morphology in subjects with untreated Class III malocclusions. *Angle Orthod* 1999;69:215–224.
65. Baumrind S, Frantz RC. The reliability of head film measurements: I. Landmark identification. *Am J Orthod* 1971a;60:111–127.
66. Sekiguchi T, Savara BS. Variability of cephalometric landmarks used for face growth studies. *Am J Orthod* 1972;61:603–618.
67. Cohen AM. Uncertainty in cephalometrics. *Br J Orthod* 1984;11:44–48.

68. El-Mangoury NH, Shaheen SI, Mostafa YA. Landmark identification in computerized posteroanterior cephalometrics. *Am J Orthod Dentofac Orthop* 1987;91:57–61.
69. Macri V, Wenzel A. Reliability of landmark recording on film and digital lateral cephalograms. *Eur J Orthod* 1993;15:137–148.
70. Major PW, Johnson DE, Hesse KL, Glover KE. Landmark identification error in posterior anterior cephalometrics. *Angle Orthod* 1994;64:447–454.
71. Nimkarn Y, Miles PG. Reliability of computer-generated cephalometrics. *Int J Adult Orthod Orthognath Surg* 1995;10:43–52.
72. Ferrario VF, Sforza C, Puleo A, Poggio CE, Schmitz JH. Three-dimensional facial morphometry and conventional cephalometrics: A correlation study. *Int J Adult Orthod Orthognath Surg* 1996a;11:329–338.
73. Kragstov J, Bosch C, Gyldensted C, Sindet-Pedersen S. Comparison of the reliability of craniofacial anatomic landmarks based on cephalometric radiographs and threedimensional CT scans. *Cleft Palate Craniofac J* 1997;34:111–116.
74. Trpkova B, Major P, Prasad N, Nebbe B. Cephalometric landmarks identification and reproducibility: A meta-analysis. *Am J Orthod Dentofac Orthop* 1997;112:165–170.
75. Nanda RS, Ghosh J, Bazakidou E. Three-dimensional facial analysis using a video imaging system. *Angle Orthod* 1996;66:181–188.
76. Altobelli DE, Kikinis R, Mulliken JB, Cline H, Lorensen W, Jolesz F. Computer assisted three-dimensional planning in craniofacial surgery. *Plast Reconstr Surg* 1993;92:576–585.
77. Spolyar JL, Vasileff W, MacIntosh RB. Image corrected cephalometric analysis (ICCA): Design and evaluation. *Cleft Palate Craniofac J* 1993;30:528–539.
78. Ferrario VF, Sforza C, Poggio CE, Schmitz JH, Tartaglia G. A three-dimensional noninvasive study of head flexion and extension in young non-patient subjects. *J Oral Rehabil* 1997;24:361–368.
79. Sarver DM, Johnston MW. Orthognathic surgery and aesthetics: Planning treatment to achieve functional and aesthetic goals *Br J Orthod* 1993;20:93–100.
80. Xia J, Samman N, Yeung RWK, Wang D, Shen SGF, Ip HHS, Tideman H. Computer-assisted three-dimensional surgical planning and simulation. 3D soft tissue planning and prediction. *Int J Oral Maxillofac Surg* 2000;29:250–258.
81. Kajikawa Y. Changes in soft tissue profile after surgical correction of skeletal Class III malocclusion. *J Oral Surg* 1979;37:167–174.
82. Ngan P, Hägg U, Yiu C, Merwin D, Wei SH. Soft tissue and dentoskeletal profile changes associated with maxillary expansion and protraction headgear treatment. *Am J Orthod Dentofac Orthop* 1996;109:38–49.
83. Corruccini RS. Shape in morphometrics: Comparative analysis. *Am J Phys Anthropol* 1987;73:289–303.
84. Ferrario VF, Sforza C, Miani A Jr, Serrao G. A three-dimensional evaluation of human facial asymmetry. *J Anat* 1995;186:103–110.
85. Ferrario VF, Sforza C, Schmitz JH, Miani A Jr, Taroni G. Fourier analysis of human soft tissue facial shape: Sex differences in normal adults. *J Anat* 1995;187:593–602.
86. Ferrario VF, Sforza C, Poggio CE, D'Addona A, Taroni A. Fourier analysis of cephalometric shapes. *Cleft Palate Craniofac J* 1996;33:206–212.
87. Ferrario VF, Sforza C, Schmitz JH, Miani A, Serrao G. A three-dimensional computerized mesh diagram analysis and its application in soft tissue facial morphometry. *Am J Orthod Dentofac Orthop* 1998;114:404–413.
88. Bookstein FL. A statistical method for biological shape comparisons. *J Theor Biol* 1984;107:475–520.
89. Ferrario VF, Sforza C, Pizzini G, Vogel G, Miani A. Sexual dimorphism in the human face assessed by Euclidean distance matrix analysis. *J Anat* 1993a;183:593–600.
90. Rohlf FJ, Marcus LF. A revolution in morphometrics. *TREE* 1993;8:129–132.
91. Read DW, Lestrel PK. Comment on uses of homologous-point measures in systematics: A reply to Bookstein et al. *Syst Zool* 1986;35:241–253.
92. Richtsmeier JT, Cheverud JM, Lele S. Advances in anthropological morphometrics. *Ann Rev Anthropol* 1992;21:283–305.